Biointerface Research in Applied Chemistry
Open-Access Journal (ISSN: 2069-5837)

Article
Volume 13, Issue 6, 2023, 579
https://doi.org/10.33263/BRIAC136.579

Normal Internal Coordinates and Harmonic Force Fields of Benzoylecgonine, Main Cocaine Metabolite. Complete Vibrational Assignments

Elida Romano [1], Davide Romani [2], Silvia Antonia Brandán [1,*]

[1] General Chemistry, Institute of Inorganic Chemistry, Faculty of Biochemistry. Chemistry and Pharmacy, National University of Tucumán, Ayacucho 471, (4000) San Miguel de Tucumán, Tucumán, Argentina; elida.romano@gmail.com (E.R.);
[2] Department of Surgical Medical Sciences and Neurosciences, University of Siena, Via Banchi di Sotto 55 (53100), Siena, Italy; dromaniti@gmail.com (D.R.);
* Correspondence: sbrandan@fbqf.unt.edu.ar (S.A.B.);

Scopus Author ID 6602262428
Received: 10.11.2022; Accepted: 9.01.2023; Published: 29.03.2023

Abstract: B3LYP/6-311++G** calculations of the main metabolite of cocaine, benzoylecgonine (BZ) as free base and in its R and S forms have been used together with normal internal coordinates, transferable scaling factors, and harmonic force fields in order to perform its complete vibrational assignments. Identification of this metabolite is important because it is detected in the urine for a minimum of 5 days after its use and can remain for four months until its complete elimination. Both forms were optimized in different environments evidencing higher solvation energy in water (-85.79 kJ/mol) than cocaine (-70.21 kJ/mol), with values closer to heroin (-88.67 kJ/mol). Structural, electronic, topological, and vibrational properties were predicted for those species in both media. Natural bond orbital studies and the atoms in molecules calculations reveal lower values in solution stabilities and topological properties. Gap values suggest that both species are less reactive in solution but both most reactive than cocaine, heroin, morphine, and scopolamine in both media. Comparisons between experimental NMR, vibrational, and electronic spectra with the corresponding predicted calculations show very good concordances. The vibrational assignments observed for the two forms indicate that both species are probably present in both phases.

Keywords: benzoylecgonine; force fields; molecular structure; frontier orbital; DFT calculations.

1. Introduction

The main metabolite formed by hydrolysis of alkaloid cocaine is benzoylecgonine which is detected in the urine for a minimum of 5 days after its use [1-7]. A very important date to keep in mind is that benzoylecgonine can remain in the body until its complete elimination after four months [1-7]. Its identification is very important not only for forensic science due to adulterations but also for human health since it is a drug of abuse that produces many consequences with frequent use [8-15]. Currently, many techniques are used for its detection, vibrational spectroscopy being one of the fastest and safest [11-15]. The latest technique requires performing the complete assignments of infrared and Raman spectra and knowing benzoylecgonine's experimental structures as free bases in its R and S forms [16,17]. The IUPAC name of benzoylecgonine is 3-Benzoyloxy-8-methyl-8-azabicyclo[3.2.1]octane-

4-carboxylic acid. So far, the complete vibrational assignments of many tropane alkaloids, such as benzoylecgonine, remain absent because all tropane alkaloids have a bicyclic (N-methyl-8-a-zabicyclo[3.2.10]octane) structure with two fused piperidine and pyrrolidine ring whose normal internal coordinates are very difficult to build. Our investigation group reported the vibrational analyses for the free base, cationic, and hydrochloride species of some tropane alkaloids combining the vibrational spectra with theoretical calculations [18]. In these cases, the vibrational spectra are predicted using DFT calculations. Later, the complete assignments are performed by comparing experimental spectra with the corresponding predicted by using the harmonic force field and the Molvib program [19-21]. As benzoylecgonine has a chiral center, in this work, its two R and S forms of its free base species were optimized at the B3LYP/6-311++G** method in the gas phase and water [22,23]. To apply the SQMFF methodology, the normal internal coordinates, transferable scaling factors, and the Molvib program are necessary to obtain the correct harmonic force fields and the potential energy distribution (PED) [19-21]. Hence, the vibration modes are assigned according to the higher PED contributions. In general, to perform the assignments of experimental bands observed to the predicted normal modes of vibration, only contributions of PED ≥ 10 are considered [19-21]. In addition, for the two R and S free base species of benzoylecgonine, the vibrational, structural, and topological properties were also predicted and compared with those reported for the corresponding to cocaine because the activating CH_3 group is present in cocaine instead of an H atom in benzoylecgonine. Chemically, cocaine is a carboxylate (methyl (3S)-3-(benzoyloxy)-8-methyl-8-azabicyclo[3.2.1]octane-2-carboxylate), while benzoylecgonine is an acid. As cocaine and all tropane alkaloids, benzoylecgonine has the tertiary nitrogen atom belonging to >N-CH_3 group related to pharmacological and medicinal properties [24-26].

2. Materials and Methods

The GaussView program was employed to remove the CH_3 group from the previously optimized R free base structure of cocaine by applying the B3LYP/6-31G* method to have the initial structure of the free base of benzoylecgonine [27,28]. Subsequently, the two structures R and S of benzoylecgonine were optimized with the Gaussian 09 program employing hybrid calculations B3LYP/6-311++G** both in the gas phase and in the aqueous solution. [22,23,29]. In both optimized structures, chair structures are observed in the piperidine rings, as in cocaine and scopolamine species [18,27]. The solvent effects were considered for all calculations in solution with the self-consistent reaction field (SCRF) method and the integral equation formalism variant polarised continuum (IEFPCM) model [30-32]. The universal solvation model was used to obtain the solvation energies of two forms of benzoylecgonine in an aqueous solution, while the variations of volumes were computed at the same level of theory the as the Moldraw program [32,33]. The harmonic force fields were calculated taking into account the normal internal coordinates, transferable scaling factors, and the SQMFF methodology with the Molvib program [18-20]. The normal internal coordinates were similar to those reported for cocaine [27]. Structural and topological properties were predicted by natural atomic population (NPA) and Merz-Kollman (MK) charges natural bond orbital (NBO), and atoms in molecules (AIM) calculations [34-37]. In contrast, the reactivities and behaviors of two benzoylecgonine species were predicted using the frontier orbitals and some descriptors [18,27]. Comparisons between experimental and theoretical NMR and UV-visible spectra are necessary in order to see correlations in the structures in both media. Hence, the ^{1}H and ^{13}C-NMR spectra of both forms of benzoylecgonine were predicted in an aqueous solution by using

gage-invariant LCAO (linear combination of atomic orbitals) method [38], while the ultraviolet-visible spectrum in the same solvent was predicted using Time-dependent DFT calculations (TD-DFT) at the same level of theory with the Gaussian 09 program [29].

3. Results and Discussion

3.1. Optimizations in both media.

Figure 1 presents the comparison of the R-free base structures of cocaine and its main metabolite, benzoylecgonine (BZ). The red circle indicates the CH_3 group present in cocaine but not in benzoylecgonine.

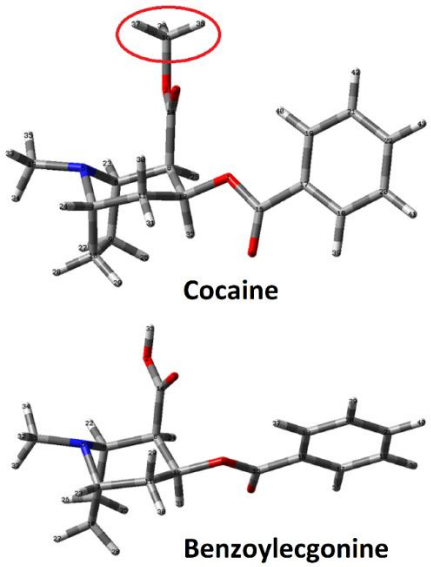

Figure 1. Molecular theoretical structures of R free base species of benzoylecgonine alkaloid compared with the corresponding to cocaine. The red circle on the CH_3 group shows the difference between both.

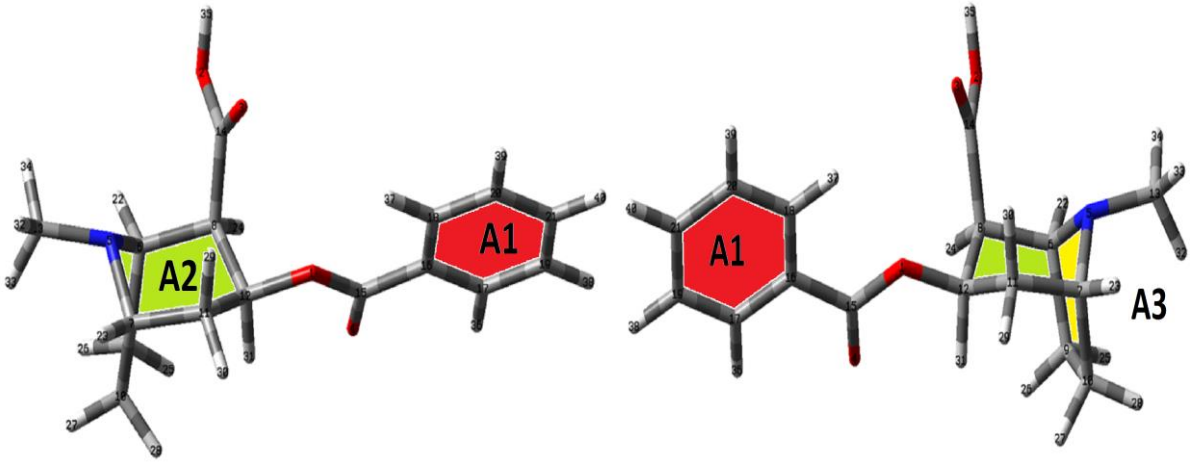

Figure 2. Molecular theoretical structures of R and S free base of benzoylecgonine showing the benzyl, piperidine, and pyrrolidine rings identified by different colors. A1 (red), A2 (green), and A3 (yellow) correspond to benzyl, pyrrolidine, and pyrrolidine rings, respectively.

The two R and S free base species of benzoylecgonine are shown in Figure 2, with their rings in distinct colors. Thus, A1 in red color corresponds to the benzyl ring while the fused piperidine (A2) ring in green color and pyrrolidine (A3) ring in yellow color, both belonging to the (N-methyl-8-a-zabicyclo[3.2.10]octane) system. The results of total energies, dipole

moments, volume variation, and solvation energy for the two forms of the free base can be seen in Table 1. The solvation energies are also presented in the table. Regarding the table values, we observed that both forms of BZ present the same energies and dipole moment values. However, little differences in the volumes are observed. Thus, the R forms in both media show a higher V value with a slight increase from 305.0 $Å^3$ in the gas phase to 307.2 $Å^3$ in the solution.

Table 1. Calculated total energies (*E*), dipole moments (μ), volume variations (ΔV), and corrected solvation energies (ΔG_c) of the R and S forms of the free base of benzoylecgonine in the gas phase and aqueous solution by using the B3LYP/6-311++G** method.

B3LYP/6-311++G Method**				
Benzoilecgonine				
Gas phase				
Species	E (Hartrees)	μ (D)	V ($Å^3$)	
Form R	-977.0880	1.5412	305.0	
Form S	-977.0880	1.5410	302.4	
Aqueous Solution				
Species	E (Hartrees)	μ (D)	V ($Å^3$)	ΔV ($Å^3$)
Form R	-977.1110	1.7832	307.2	2.2
Form S	-977.1110	1.7819	302.6	0.2
Solvation energy (kJ/mol)				
Species	ΔG_{un}	ΔG_{ne}	ΔG_c	
Form R	-60.33	25.46	-85.79	
Form S	-60.33	25.46	-85.79	

ΔG_{un}, See text.

Analyzing the orientations, directions, and magnitudes of dipole moment vectors of both forms of BZ from Figure S1, it is observed that the magnitudes are practically the same in the two media (1.54 D in the gas phase and 1.78 D in the solution). However, the orientations and directions slightly change in solution, although the vectors of both R and S forms in the two media are directed toward the tertiary N atoms. This work used the Moldraw program to calculate the volume variations [33]. When the V values are compared with the obtained for the R form of cocaine in both media (321.0 $Å^3$ in gas phase and 322.2 $Å^3$ in solution) by using hybrid B3LYP/6-31G* calculations, we observed higher volumes in cocaine, as expected because this alkaloid present a CH_3 group different from BZ. The dipole moment values in cocaine change from 1.55 D in the gas phase to 1.88 D in solution with a V expansion of 1.2 $Å^3$. Hence, the absence of the CH_3 group in BZ generates higher V expansion and, as a consequence, both R and S forms of BZ show higher solvation energies (-85.79 kJ/mol) than cocaine (-70.21 kJ/mol). Comparing the solvation energies of both forms of BZ with the corresponding scopolamine (-75.47 kJ/mol), heroin (-88.67 kJ/mol), and morphine (-60.91 kJ/mol), predicted by using B3LY/6-31G* calculations, we observed that the values are closer to heroin [18,27]. Probably, BZ remains in the body until its complete elimination after four months due to its higher solubility in water. Here, the uncorrected (ΔG_{un}) solvation energies are calculated as the differences between E in solution and E gas phase. For instance, the value of -85.79 kJ/mol for the form R is calculated from ΔG_{un} = [-977.1110-(-977.0880)] x 627.51 x 4.18= -60.33 kJ/mol. Then, the corrected solvation energies (ΔG_c) are calculated as the differences between the uncorrected values (-60.33 kJ/mol) and the non-electrostatic terms due to the cavitation, dispersion, and repulsion energies (25.46 kJ/mol) computed with the universal solvation modes from the SCRF calculations [30-32]. Note that free bases of cocaine and BZ undergo volume expansion in solution because they are basic species that are hydrated in

solution. Probably, the higher solvation energy observed for BZ than cocaine supports its permanence in the human organism for four months.

3.2. Geometrical parameters in both media.

Comparisons of calculated geometrical parameters for the R and S forms of the free base of BZ in the gas phase and aqueous solution applying the hybrid B3LYP/6-311++G** method with the corresponding experimental ones for freebase cocaine [16] and ecgonine hydrochloride [17] are summarized in Table 2.

Table 2. Comparisons of calculated geometrical parameters for the R and S forms of benzoylecgonine in gas and aqueous solution phases with the corresponding experimental ones for freebase cocaine and ecgonine hydrochloride.

Parameters	B3LYP/6-311++G** Method[a]				Exp[b]	Exp[c]
	Form R		Form S			
	Gas	Solution	Gas	Solution		
Bond lengths (Å)						
N5-CH_3	1.461	1.470	1.461	1.470	1.468	1.490
N5-C6	1.473	1.479	1.473	1.479	1.460	1.514
N5-C7	1.478	1.485	1.478	1.485	1.467	1.511
C6-C9(A5)	1.560	1.556	1.560	1.556	1.522	1.537
C7-C10(A5)	1.560	1.556	1.560	1.556	1.527	1.536
C6-C8(A6)	1.557	1.559	1.557	1.559	1.531	1.540
C7-C11(A6)	1.541	1.539	1.541	1.539	1.531	1.524
C8-C12(A6)	1.540	1.541	1.540	1.541	1.518	1.553
C11-C12(A6)	1.528	1.527	1.528	1.527	1.512	1.527
C12-O1	1.446	1.459	1.446	1.459	1.450	1.420
C15=O4	1.213	1.221	1.213	1.221	1.193	-
C15-O1	1.350	1.343	1.350	1.343	1.329	-
C14-O2	1.363	1.352	1.363	1.352	1.333	1.320
C14=O3	1.203	1.215	1.203	1.215	1.188	1.214
O2-H35	0.969	0.972	0.969	0.972	-	0.859
C15-C16	1.491	1.488	1.491	1.488	1.499	-
RMSD[b]	**0.021**	**0.021**	**0.021**	**0.021**		
RMSD[c]	**0.039**	**0.038**	**0.039**	**0.038**		
Bond angles (°)						
C13-N5-C6	114.0	112.0	114.0	112.0	112.6	112.9
C13-N5-C7	114.2	112.5	114.2	112.5	113.1	113.5
C6-N5-C7(A5,A6)	101.9	101.3	101.9	101.3	100.9	102.1
N5-C6-C9(A5)	105.4	105.4	105.4	105.4	106.2	102.3
N5-C7-C10(A5)	104.8	105.1	104.8	105.1	105.4	102.8
C6-C9-C10(A5)	103.7	103.8	103.7	103.8	103.5	105.2
N5-C6-C8(A6)	106.9	108.4	106.9	108.4	106.8	108.5
N5-C7-C11(A6)	107.7	107.8	107.6	107.8	106.7	106.8
C8-C12-C11(A6)	112.4	113.4	112.4	113.4	112.2	111.7
C12-O1-C15	117.5	118.3	117.5	118.3	117.7	-
C14-O2-H35	106.7	108.6	106.7	108.6	-	107.2
O4-C15-C16	124.3	123.7	124.3	123.7	124.8	-
RMSD[b]	**0.77**	**0.88**	**0.76**	**0.88**		
RMSD[c]	**1.47**	**1.59**	**1.47**	**1.59**		
Dihedral angles (°)						
C8-C6-N5-CH_3(A6)	160.1	164.6	-160.1	-164.7	160.6	164.5
C11-C12-O1-C15	151.6	149.8	-151.6	-149.8	-139.0	-
C12- C8-C14-O2	170.9	159.1	-170.9	-159.1	179.4	99.6
C16-C15-O1-C12	179.6	-178.8	-179.6	178.8	178.1	-
O4-C15-O1-C12	-0.4	1.2	0.4	-1.2	-1.3	-
C8-C12-O1-C15	-83.3	-84.5	83.4	84.4	96.3	-

[a]This work, [b]Ref [39] for freebase cocaine; [c]Ref [40] hydrochloride ecgonine; A6, six member's ring (piperidine); A5, five member's ring (pyrrolidine).

These comparisons were performed using the root mean square deviation (RMSD) values. Hence, better correlations for the bond lengths and angles of both forms in the two

media are observed with the values of cocaine [16], showing for the distances an RMSD value of 0.021 Å while by using the experimental value of ecgonine hydrochloride [17] the RMSD values increase a few to 0.039-0.038 Å. Here, the most interesting results are observed for the C14=O3 and O2-H35 bonds because, in cocaine, the bond length C14=O3 is 1.188 Å while these distances in the two forms of BZ are predicted between 1.215 and 1.203 Å. These enlargements of bonds are attributed to activating the CH_3 group present in cocaine, while in BZ is the H atom that is less linked to O2. Other interesting comparisons are observed in the bond lengths of N5-CH_3, which is present in all tropane alkaloids. The values for BZ are closer to cocaine values [16] but different from the observed for ecgonine hydrochloride [17]. For the bond, angles are observed in a similar situation. Thus, when the predicted values are compared with the corresponding cocaine values [16], RMSD values are observed between 0.88 and 0.76°, while by using the other reference [17], the RMSD values increase to 1.59-1.47°. In relation to the dihedral angles, they show higher differences between the R and S forms, as expected, because the dihedral C8-C6-N5-CH_3 (A6) and C12-C8-C14-O2 angles in the S form present negative signs while in the R forms positive ones. Hence, the R forms of BZ in both media show dihedral C8-C6-N5-CH_3 values closer to corresponding to experimental A6 six member's ring of piperidine of hydrochloride ecgonine [17]. Still, different values for dihedral C12-C8-C14-O2 angles are observed. The low RMSD values predicted for bond lengths and angles suggest that both R and S structures of BZ can be used in the vibrational analyses to perform their complete assignments using the harmonic force fields calculated from SQMFF methodology [19-21].

3.3. Charges, molecular electrostatic potentials, and bond order studies.

Atomic natural population (NPA) and Merz-Kollman (MK) charges, together with the molecular electrostatic potentials (MEP) and bond orders (BO) for the R and S forms of BZ, are studied in this section. Table S1 of Supporting material shows the MK charges and the MEP values because these charges are used to predict the MEP values [34]. Table S2 shows the NPA and BO values for the two forms of BZ by using B3LYP/6-311++G** calculations.

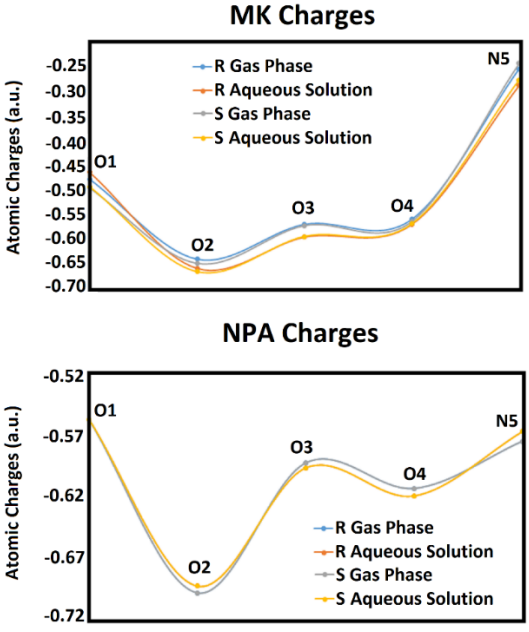

Figure 3. Calculated Merz-Kollman (MK) and natural population atomic (NPA) charges of both R and S free base species of benzoylecgonine by using the B3LYP/6-311++G** method

Both tables show the mentioned properties on all atoms of both species and in the two media, while Figure 3 are presented only the values observed for the acceptors and donor's groups of H bonds. Thus, the O1, O2, O3, O4, and N5 atoms are involved in forming H bonds in the solution.

Figure 3 shows on those atoms negative MK and NPA charges, but different values are observed because the MK charges show variations from -0.25 to -0.70 a.u., while the NPA only variations from -0.56 to -0.70 a.u. Hence, lower variations are observed in the NPA charges. Both charges on O2 belonging to O2-H35 bonds present the most negative values, while the H35 atoms have the higher positive values because these atoms are the most labile, as supported by the low MEP values. Figure 3 evidence that both charges present few changes in the solution. On the other side, on C atoms of piperidine and pyrrolidine rings of R and S forms, different MK and NPA charges are observed (in Table S1) because positive MK charges are observed on C7 and C12 of R and S forms in both media while the NPA charges on C6 and C12 of R and S forms show positive charges. Very important results are observed in the NPA charges on N5 of both forms because their values decrease in solution, indicating that these atoms of R and S species could be hydrated in this medium. On the contrary, the MK on N5 of the two forms in both media evidences the most negative values.

When MEP values are analyzed for all atoms from Table S1, the tendency observed is expected due to the different electronegativities: O > N > C >H. The most labile atoms that have less negative MEP values are the H35 atoms of O2-H35 bonds, as previously mentioned. In solution, the values on H35 decrease, indicating these atoms are involved in the formation of H bonds in both species. We can see the nucleophilic and electrophilic sites by analyzing the mapped MEP surfaces through different red and blue colorations shown in Figure S2. Thus, the nucleophilic sites are observed on the O atoms corresponding to the COO groups and N atoms of both free bases species, while blue colors are on the H atoms. Green colors are observed on the inert sites.

Regarding the bond orders (BO), expressed as Wiberg indexes from Table S2, it is observed only slight differences in the BO related to C13 and C14 corresponding to the piperidine and COOH of both species of BZ, respectively, while the H35 atoms present the lower values because they have higher lability, as supported by the low MEP values.

3.4. NBO and AIM calculations.

The two R and S forms of BZ evidence higher solvation energies than cocaine, and for this reason, knowing its stabilities in both media are very important to justify why staying longer in the human body. Here, these studies were performed by using NBO and AIM calculations [35-37]. In the first case, the E(2) parameters are calculated as donor-acceptor energy interactions obtained from the second-order perturbation theory analysis of the Fock matrix with the NBO 3.1 program by using the hybrid B3LYP/6-311++G** method [35]. Main donor-acceptor energies for the R and S forms of BZ in the gas phase and aqueous solution by using the hybrid B3LYP/6-311++G** level of theory can be seen in Table S3. Regarding the table, we observed the same four transitions in both species and the two media, which are the $\pi \rightarrow \pi^*$, $\pi^* \rightarrow \pi^*$, $n \rightarrow \sigma^*$ and $n \rightarrow \pi^*$ interactions. The first $\pi \rightarrow \pi^*$ interactions are related to the charges transfer from bonding orbital C=C to antibonding C=C of benzyl ring, other corresponds to the only $\pi^*O4\text{-}C15 \rightarrow \pi^*C16\text{-}C18$ interaction while the other two are related to transitions from lone pairs of O3 and O4 towards different antibonding σ^* and π^* orbitals.

Note that the $\pi \rightarrow \pi^*$ interactions of both species in the two media present higher values. Evaluating total energies, we observed that the two forms are less stable in an aqueous solution (1803.79 kJ/mol) than in the gas phase (1836.02 kJ/mol). The R free base species of cocaine has also evidenced three interactions ($\pi \rightarrow \pi^*$, $\pi^* \rightarrow \pi^*$ and $n \rightarrow \sigma^*$) and lower stability in solution but with a total energy value of 1824.32 kJ/mol by using the hybrid B3LYP/6-31G* level of theory [27]. Obviously, the differences observed are related to the additional CH_3 group in cocaine and the lower basis set used.

The stabilities of two species of BZ were also studied, analyzing the possible intra-molecular interactions from the theory of atoms in molecules (AIM) using the topological properties calculated with the AIM 2000 program [36,37]. Hence, the electron density, $\rho(r)$, the Laplacian values, $\nabla^2\rho(r)$, the eigenvalues $(\lambda 1, \lambda 2, \lambda 3)$ of the Hessian matrix and the $|\lambda 1|/\lambda 3$ ratio are calculated in the bond critical points (BCPs) and ring critical point (RCP). Table S4 shows the results for the two species of BZ by using the hybrid B3LYP/6-311++G** level of theory. Both forms show the same topological properties in the two media with the formation of new H bonds and new RCPs, the C14-O3···H29 in the R forms and the C14-O3···H30 bonds in the S forms and new RCPNs. The molecular graphics for both species in the gas phase showing the H bonds and RCPNs are given in Figure 4, while Figure S3 shows the molecular graphics for the two forms of BZ in both media.

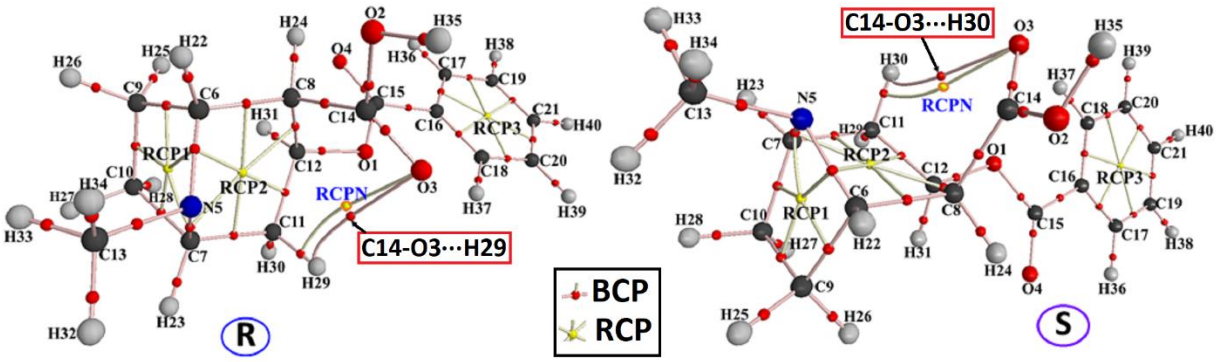

Figure 4. Molecular graphics of two species of benzoylecgonine in gas phase displaying their H bonds interactions (BCPs) and ring critical points (RCPs) at B3LYP/6-311++G** level of theory.

The topological properties slightly decrease in solution, as observed in Table S4, while Figure S3 shows the proximities between the BCPs (red colors) and the RCPNs (yellow colors). When the densities of the three different benzyls, piperidine, and pyrrolidine ring named RCP1, RCP2, and RCP3, respectively, are analyzed, we see that the piperidine rings have the lowest values while the highest values are observed in the pyrrolidine rings, as was also observed in cocaine [27]. Besides, in the R form of freebase cocaine, H bond interaction was predicted in the two media but with higher topological properties than BZ [27].

3.5. Frontier orbitals and descriptors studies.

Here, the reactivities of R and S forms of BZ are predicted together with some descriptors in both media by the B3LYP hybrid level of theory using the basis set 6-311++G** because Pauling and Datta [39] predicted anticholinergic activities for all tropane alkaloids. The difference between the highest occupied molecular orbital (HOMO) and the lowest unoccupied molecular orbital (LUMO) is known as gap energy and, in particular, when its value is low, the species is reactive, while a high gap value indicates that it is less reactive

probably due to its higher kinetic stability. Table S5 shows calculated HOMO and LUMO orbitals, energy band gap, chemical potential (μ), electronegativity (χ), global hardness (η), global softness (S), and global electrophilicity index (ω) for the R and S forms of BZ in the two media by using the same method mentioned above. At the bottom of table S5, the equations used to calculate the descriptors are presented. R and S species are less reactive in solution because the gap values are higher than those observed in the gas phase. When the gap values for both forms of BZ are compared with R forms of cocaine in both media (-4.858 eV in gas phase and -4.9487 eV in aqueous solution), we observed that cocaine is less reactive in both media than the two species of BZ probably due to activating CH3 group present in cocaine. Comparing the gap values of both forms of BZ with the corresponding to other alkaloids such as scopolamine (5.4004 and 5.4758 eV, respectively, in the gas phase and solution), heroin (5.6563 and 5.6414 eV, respectively, in the gas phase and solution) and morphine (5.6044 and 5.4750 eV, respectively in gas phase and solution), it is observed that the two species of BZ are most reactive than the other alkaloids and, specifically in solution [18,27]. The lower reactivities of both species of BZ probably allow these species to remain in the human body for a long time. In relation to the descriptors, $> \chi > \mu > S > \omega$ and $< \eta$ are observed for the less reactive R and S species in solution.

3.6. NMR study.

Correlations between experimental and theoretical structures of BZ are analyzed by comparing 1H and 13C-NMR chemical shifts of the R and S forms by applying the root mean square deviation (RMSD) values. These analyses are very important to produce the vibrational analyses with the two optimized structures of BZ by using B3LYP/6-311++G** calculations.

Table 3. Calculated ^{1}H chemical shifts (δ in ppm) for benzoylecgonine in aqueous solution by using the B3LYP/6-311++G** method compared with the corresponding experimental in CD_3CN solution.

^{1}H-NMR[a]				
H Atoms	**6-311++G****		**Experimental in CD_3CN[b]**	
	R	**S**	**δ ppm**	**Integ. Multiplicity (JHz)**
H22	3.67	3.67	3.71	1H dd (3.1; 6.1)
H23	3.34	3.34	3.64	1H dt (6.4; 3.1; 3.1)
H24	3.45	3.46	2.99	1H dd (3.1)
H25	1.73	**2.32**	2.26	1H dd (9.8; 6.1)
H26	2.32	**1.73**	1.89	1H t (9.8; 9.8)
H27	2.15	**1.54**	2.26	1H dd (9.8; 6.4)
H28	1.54	**2.15**	1.96	1H t (9.8; 9.8)
H29	2.39	**1.89**	2.33	1H ddd (13.5; 11.3; 3.1)
H30	1.89	**2.39**	2.14	1H ddd (13.5; 6.5; 3.1)
H31	5.50	5.50	5.32	1H dt (11.3; 6.5; 6.5)
H32	2.26	2.26	2.54	3H s
H33	2.12	2.12		
H34	2.19	2.19		
H35	7.10	7.10	-	-
H36	8.55	8.55	7.96	2H dd (8.5; 1.4)
H37	8.44	8.44		
H38	7.88	7.88	7.48	2H dd (8.5; 7.3)
H39	7.89	7.89		
H40	8.03	8.03	7.61	1H tt (7.3; 1.4)
RMSD	**0.36**	**0.37**		

[a]This work GIAO/B3LYP/6-311++G** Ref. to TMS, [b]From Ref [7]. In bold letters are shown the differences between both R and S forms.

Hence, Tables 3 and 4 summarize calculated 1H and 13C-NMR chemical shifts for the R and S forms of BZ in an aqueous solution compared with the corresponding experimental for benzoylecgonine in CD3CN solution reported by Pedersoli *et al*. [7].

NMR chemical shifts were predicted for both species of BZ in an aqueous solution by using a gage-invariant LCAO method reported by Ditchfield [38]. Table 3 shows very good correlations for both forms of BZ with RMSD values between 0.37 and 0.36 ppm. Note that the values corresponding to H nuclei of CH_2 groups identified by C9, C10, and C11 of the R form are predicted to be exchanged for the S form. These values are indicated in Table 3 by letter bold. CH_2 groups identified by C9 and C10 belong to the piperidine ring, while the group identified by C11 belongs to the pyrrolidine ring.

Table 4. Calculated ^{13}C chemical shifts (δ in ppm) for benzoylecgonine in an aqueous solution by using the B3LYP/6-311++G** method compared with the corresponding experimental in CD_3CN solution.

^{13}C-NMR[a]			
C Atoms	**6-311++G****		**Experimental[b]**
	R	**S**	**δ ppm**
6	70.8	70.8	65.3
7	66.4	66.4	61.9
8	53.2	53.2	49.3
9	28.2	28.2	24.6
10	26.6	26.6	25.7
11	37.9	37.9	34.6
12	74.3	74.3	66.3
13	40.6	40.6	38.5
14	183.9	183.9	174.0
15	174.9	174.9	166.4
16	134.3	134.3	131.2
17	136.2	136.2	130.4
18	135.4	135.4	
19	133.9	133.9	129.6
20	134.1	134.1	
21	140.7	140.7	134.2
RMSD	**5.47**	**5.47**	

[a]This work GIAO/B3LYP/6-31G* Ref. to TMS, [b]From Ref [7]

Regarding the correlations between experimental [7] and calculated ^{13}C chemical shifts from Table 4, we see that the RMSD values are the same for the R and S species but slightly higher than the H ones (5.47 ppm). These differences could be associated with the B3LYP/6-311++G** calculations because this calculation level produces better results for the H nuclei than the C ones and could also be attributed to solvent because the chemical shifts were predicted in aqueous solution instead CD_3CN solution. These good concordances in the RMSD suggest that both structures can perfectly be used to perform the corresponding vibrational studies and assignments of predicted infrared and Raman spectra of the R and S forms of benzoylecgonine by using the SQMFF methodology.

3.7. Vibrational analysis.

Both forms of BZ in the two media were optimized with C_1 symmetries by using the hybrid B3LYP/6-311++G** method. According to forty atoms present in both species are expected a total of 114 normal vibration modes where all modes have activity in the infrared and Raman spectra. Figures 5 and 6 show comparisons of experimental infrared and Raman spectra of BZ in the solid phase [40] with the corresponding predicted for the R and S forms in

the gas phase by using the hybrid B3LYP/6-311++G** method. Note the very good correlations between experimental and theoretical calculations.

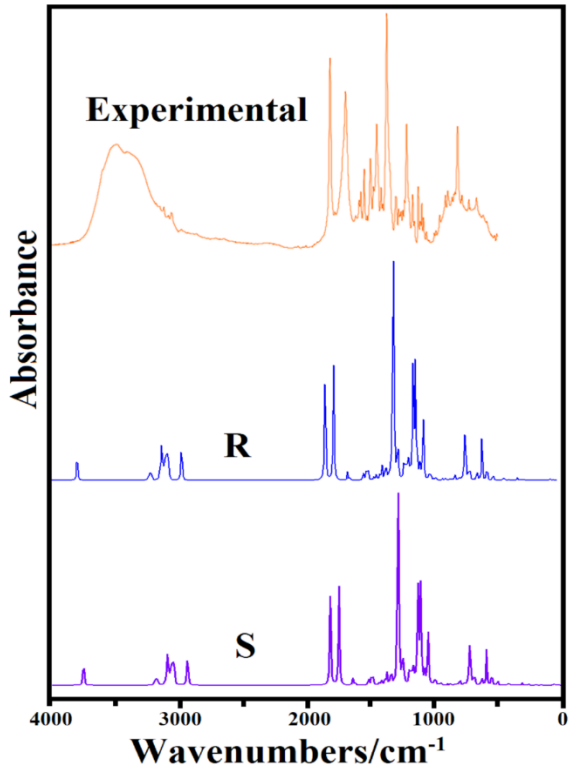

Figure 5. Comparisons between the experimental infrared spectrum of benzoylecgonine in the solid phase [40] with the corresponding predicted for the R and S form of the free base in the gas phase by using B3LYP/6-311++G** level of theory.

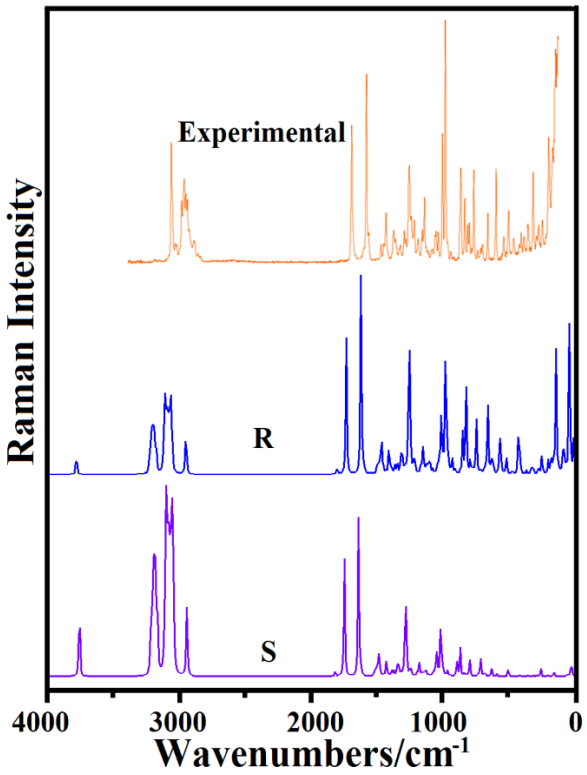

Figure 6. Comparisons between the experimental Raman spectra of benzoylecgonine in the solid phase [40] with the corresponding predicted for the R and S form of the free base in the gas phase by using B3LYP/6-311++G** level of theory.

The predicted Raman spectra were corrected from activities to intensities to obtain better correlations [41]. In the region of higher wavenumbers, the experimental IR spectrum shows the typical broadband attributed to OH stretching modes of the COOH group. Besides, the R and S forms present practically the same IR spectra. Only a few differences in the Raman spectra are observed because the S form presents higher intensities in the bands at higher wavenumbers, as shown in Figure 6. Such differences are associated with the CH_2 groups previously predicted by NMR studies. Here, to calculate the harmonic force fields with the SQMFF methodology were used the normal internal coordinates for the free base of cocaine, transferable scaling factors, and the Molvib program [19-21]. PED contributions ≥ 10 % have been used for the assignments of normal vibration modes. Observed and calculated wavenumbers for the two forms of benzoylecgonine in the gas phase and their corresponding assignments are presented in Table 5.

Table 5. Observed and calculated wavenumbers (cm^{-1}) and assignments for R and S forms of benzoylecgonine in the gas phase by using the B3LYP/6-311++G** method.

Experimental[c]		B3LYP/6-311++G** Method[a]			
		Form R		Form S	
IR	Raman	SQM[b]	Assignments	SQM[b]	Assignments
3409 m		3606	νO2-H35	3605	νO2-H35
3324 br		3079	νC18-H37	3079	νC18-H37
	3071 s	3068	νC17-H36	3068	νC17-H36
		3055	νC21-H40,νC20-H39	3055	νC21-H40,νC20-H39

Experimental[c]		B3LYP/6-311++G** Method[a]			
		Form R		Form S	
IR	Raman	SQM[b]	Assignments	SQM[b]	Assignments
Experimental[c]		B3LYP/6-311++G** Method[a]			
		Form R		Form S	
IR	Raman	SQM[b]	Assignments	SQM[b]	Assignments
	3041 w	3046	νC19-H38,νC20-H39	3046	νC19-H38, νC20-H39
3035 w	3032 w	3033	νC21-H40	3033	νC21-H40
3006 w	2994 m	2985	$\nu_a CH_2$(C11)	2985	$\nu_a CH_2$(C11)
2979 w	2973 s	2976	νC6-H22	2976	νC6-H22
	2973 s	2971	$\nu_a CH_3$	2971	$\nu_a CH_3$
	2973 s	2968	$\nu_a CH_2$(C9)	2968	$\nu_a CH_2$(C9)
	2961 m	2962	νC12-H31	2962	νC12-H31
	2950 m	2953	$\nu_a CH_2$(C10)	2953	$\nu_a CH_2$(C10)
	2950 m	2947	νC7-H23	2947	νC7-H23
	2934 sh	2936	νC8-H24	2936	νC8-H24
	2934 sh	2933	$\nu_a CH_3$	2933	$\nu_a CH_3$
	2934 sh	2931	$\nu_s CH_2$(C9)	2931	$\nu_s CH_2$(C9)
		2923	$\nu_s CH_2$(C10)	2923	$\nu_s CH_2$(C10)
	2899 w	2918	$\nu_s CH_2$(C11)	2918	$\nu_s CH_2$(C11)
	2867 vw	2821	$\nu_s CH_3$	2821	$\nu_s CH_3$
1731s	1713 s	1748	νC14=O3	1749	νC14=O3
1692 m	1713 s	1687	νC15=O4	1687	νC15=O4
1609s	1601 s	1588	νC17-C19	1588	νC17-C19
1528 w	1490 w	1568	νC19-C21, νC20-C21 νC16-C18	1568	νC19-C21,νC20-C21 νC16-C18
1504 m	1470 w	1475	βC19-H38 βC20-H39	1475	βC19-H38 βC20-H39
1488 m	1453 m	1451	δCH_2(C9), δCH_2(C10)	1451	δCH_2(C9), δCH_2(C10)
1461 m		1444	$\delta_a CH_3$	1444	$\delta_a CH_3$
		1436	βC21-H40,βC20-H39	1436	βC21-H40, βC20-H39
		1431	δCH_2(C11) δCH_2(C9)	1431	δCH_2(C11) δCH_2(C9)
		1427	$\delta_a CH_3$	1427	$\delta_a CH_3$
1414 m		1426	δCH_2(C11)	1426	δCH_2(C11)
1386 sh	1394 w	1398	ρC12-H31	1398	ρC12-H31
	1383 w	1394	$\delta_s CH_3$	1394	$\delta_s CH_3$
1364 s		1377	ρ'C8-H24,ρ'C12-H31	1377	ρ'C8-H24, ρ'C12-H31
1332 m	1343 w	1350	ρC6-H22,ρC7-H23	1350	ρC6-H22, ρC7-H23
1318 w		1338	ρ'C8-H24, wagCH_2(C11)	1338	ρ'C8-H24, wagCH_2(C11)
1320 m	1318 w	1317	wagCH_2(C11)	1317	wagCH_2(C11)
		1312	βC18-H37,βC17-H36	1312	βC18-H37,βC17-H36
	1303 w	1304	wagCH_2(C10), ρ'C7-H23	1304	wagCH_2(C10), ρ'C7-H23
		1303	ρ'C6-H22	1303	ρ'C6-H22
		1294	νC16-C17	1294	νC16-C17
1289 vs	1277 s	1292	wagCH_2(C9)	1292	wagCH_2(C9)
	1262 sh	1258	ρC6-H22,δO2-H35	1258	ρC6-H22,δO2-H35
		1248	ρC8-H24	1248	ρC8-H24
		1245	νC15-C16	1245	νC15-C16
	1239 m	1240	ρ'C6-H22, ρC7-H23	1240	ρ'C6-H22, ρC7-H23
		1222	wagCH_2(C10), wagCH_2(C9)	1222	wagCH_2(C10), wagCH_2(C9)
1214 m	1212 w	1213	ρCH_2(C10)	1213	ρCH_2(C10)
1191 w	1180 w	1208	ρCH_2(C9), ρCH_2(C11)	1208	ρCH_2(C9), ρCH_2(C11)
1174 w	1161 m	1163	βC20-H39	1163	βC20-H39
1159 w		1151	ρCH_3,ρCH_2(C10)	1151	ρCH_3,ρCH_2(C10)
		1150	βC21-H40, βC19-H38	1150	βC21-H40, βC19-H38

Experimental[c]		B3LYP/6-311++G** Method[a]			
		Form R		Form S	
IR	Raman	SQM[b]	Assignments	SQM[b]	Assignments
	1135 vw	1136	ρCH_2(C11), ρ'CH_3	1136	ρCH_2(C11), ρ'CH_3
Experimental[c]		B3LYP/6-311++G** Method[a]			
		Form R		Form S	
IR	Raman	SQM[b]	Assignments	SQM[b]	Assignments
1130 s		1127	νC11-C12	1127	νC11-C12
		1120	ρ'CH_3 ρCH_3	1120	ρ'CH_3 ρCH_3
	1105 vw	1102	νN5-C13	1102	νN5-C13
1081 m	1083 w	1095	νC15-O1	1095	νC15-O1
1069 w	1073 w	1068	νC14-O2, δO2-H35	1068	νC14-O2, δO2-H35
	1058 w	1061	νC18-C20	1061	νC18-C20
1039 m		1036	τR_1(A2),τR_2(A2)	1036	τR_1(A2), τR_2(A2)
1022 w	1028 s	1023	νN5-C7	1023	νN5-C7
		1018	βR_1(A1)	1018	βR_1(A1)
1010 w	1005 vs	1007	τR_1(A2)	1007	τR_1(A2)
		1002	γC21-H40, γC19-H38	1002	γC21-H40, γC19-H38
997 w		993	βR_1(A1), νC19-C21	993	βR_1(A1), νC19-C21
		992	γC17-H36, γC18-H37	992	γC17-H36, γC18-H37
974 vw	963 vw	967	τR_2(A2), νC12-O1	967	τR_2(A2), νC12-O1
		960	νC7-C11	960	νC7-C11
		951	γC21-H40, γC18-H37 γC17-H36	951	γC21-H40, γC18-H37 γC17-H36
	943 vw	944	βR_1(A3)	944	βR_1(A3)
		923	τ$_w$$CH_2$(C9), νC6-C8	923	τ$_w$$CH_2$(C9), νC6-C8
912 vw		910	νC6-C9, νC8-C12 νC11-C12	910	νC6-C9, νC8-C12 νC11-C12
898 vw	887 s	861	νC9-C10	861	νC9-C10
868 w	857 m	855	γC19-H38, γC20-H39	855	γC19-H38, γC20-H39
	839 m	848	δCOO(C15), δC12O1C15	848	δCOO(C15), δC12O1C15
823 m	822 m	833	τ$_w$$CH_2$(C11), νC8-C14	833	τ$_w$$CH_2$(C11), νC8-C14
805 m	805 w	809	γCOO(C15)	809	γCOO(C15)
		801	νC7-C10	801	νC7-C10
771 m	788 s	771	νN5-C6	771	νN5-C6
756 sh	762 vw	754	βR_1(A3), βR_2(A3)	754	βR_1(A3), βR_2(A3)
729 s	738 w	742	βR_2(A3), τ$_w$$CH_2$(C10)	742	βR_2(A3), τ$_w$$CH_2$(C10)
	721 w	715	γCOO(C15), γC21-H40	715	γCOO(C15), γC21-H40
		714	βR_1(A3)	714	βR_1(A3)
695 m		693	δCOO(C14)	693	δCOO(C14)
	683 m	681	βR_3(A1)	681	βR_3(A1)
		676	τR_1(A1)	676	τR_1(A1)
642 m		656	γCOO(C14)	656	γCOO(C14)
	621 s	628	βR_1(A1)	628	βR_1(A1)
	562 w	601	βR_1(A3), τR_2(A2)	601	βR_1(A3), τR_2(A2)
581 m		551	τO2-H35	551	τO2-H35
530 w	524 m	537	δCOO(C14), τR_2(A2)	537	δCOO(C14), τR_2(A2)
499 w	489 w	496	ρCOO(C15)	496	ρCOO(C15)
	459 vw	481	βR_2(A2)	481	βR_2(A2)
437 vw	446 w	441	τR_2(A1), γC16-C15	441	τR_2(A1), γC16-C15
	431 w	416	βR_3(A2)	416	βR_3(A2)
	411 w	406	τR_2(A2)	406	τR_2(A2)
	384 m	401	τR_3(A1)	401	τR_3(A1)
		367	τR_2(A2), τR_3(A2)	367	τR_2(A2,) τR_3(A2)
	337 s	346	τR_1(A2), τR_2(A2)	346	τR_1(A2), τR_2(A2)

Experimental[c]		B3LYP/6-311++G** Method[a]			
		Form R		Form S	
IR	Raman	SQM[b]	Assignments	SQM[b]	Assignments
	312 w	306	ρCOO(C14)	306	ρCOO(C14)
	299 w	283	ρN5-C13	283	ρN5-C13
Experimental[c]		B3LYP/6-311++G** Method[a]			
		Form R		Form S	
IR	Raman	SQM[b]	Assignments	SQM[b]	Assignments
	270 w	271	βC16-C15, δO1C12C11	271	βC16-C15, δO1C12C11
	223 s	252	γN5-C13	252	γN5-C13
		203	τR_1(A3), τR_2(A3)	202	τR_1(A3), τR_2(A3)
	194 s	195	δC12C8C14	195	δC12C8C14
	171 s	177	$\tau_w CH_3$	177	$\tau_w CH_3$
		159	βR_3(A2)	159	βR_3(A2)
	154s[d]	154	γC16-C15, τR_2(A1)	153	γC16-C15, τR_2(A1)
	116w[d]	119	τR_2(A2), τR_1(A2)	119	τR_2(A2), τR_1(A2)
	99m[d]	99	τR_3(A2), δC6C8C14	99	τR_3(A2), δC6C8C14
	53w[d]	55	τ_wCOO(C15)	55	τ_wCOO(C15)
		48	τ_wCOO(C14)	48	τ_wCOO(C14)
		45	τR_2(A2), τR_1(A2)	45	τR_2(A2), τR_1(A2)
	33w[d]	28	τO1-C15	28	τO1-C15
		19	τO1-C12, δO1C12C8	19	τO1-C1,2 δO1C12C8

Abbreviations: ν, stretching; β, deformation in the plane; γ, deformation out of plane; wag, wagging; τ , torsion; β_R, deformation ring τ_R, torsion ring; ρ, rocking; τw, twisting; δ, deformation; a, antisymmetric; s, symmetric; (A_1), benzyl Ring1; (A_2), piperidine Ring 2; (A_3), pyrrolidine Ring 3. [a]This work, [b]From scaled quantum mechanics force field; [c]From Ref [40]; [d]From Ref [42].

Clearly, the same assignments evidenced for the R and S forms show that both species are present in the solid phase. Then, only assignments for some groups are discussed briefly below.

3.7.1. 4000-2000 cm^{-1} region.

The IR band of medium intensity at 3409 cm^{-1} is assigned to O-H stretching modes [43,44], while the shoulder at 3324 cm^{-1} and the group of Raman bands between 3071 and 2973 cm^{-1} can be assigned to aromatic CH stretching modes of benzyl rings in agreement with that reported in the literature [45,46,47]. In the free base of cocaine, the aromatic CH stretching mode is predicted between 3108 and 3053 cm^{-1}, while the aliphatic ones are between 3035 and 2942 cm^{-1} [27]. The Raman band and shoulder at 2950 and 2934 cm^{-1}, respectively, are assigned to the aliphatic CH stretching modes (C7-H23 and C8-H24). Antisymmetric and symmetric stretching modes of methyl and methylene groups [48] are assigned as predicted by SQM calculations.

3.7.2. 2000-1000 cm^{-1} region.

The two intense IR and Raman bands at 1713 and 1692 cm^{-1} are assigned to C14=O3 and C14=O4 stretching modes, while the group of bands between 1601 and 1490 cm^{-1} is attributed to C=C of benzyl rings [44, 49, 50, 51]. The CH_3 deformation modes in cocaine are predicted between 1474 and 1409 cm^{-1}, while in BZ, they are predicted between 1444 and 1394 cm^{-1} [27]. They are assigned in these regions [45, 46, 52], as detailed in Table 5. The deformation, wagging, rocking, and twisting modes of CH_2 groups in cocaine are predicted in the 1483/1449, 1382/1242, 1230/1167, and 933/744 cm^{-1} regions [27], while in both species of

BZ, they are predicted respectively in 1451/1426, 1317/1222, 1213/1136 and 923/742 cm^{-1}, in accordance with the reported for molecules containing similar groups [53,54,55].

3.7.3. 1000-100 cm^{-1} region.

In this region, the N5-CH_3 stretching modes are important because they are present in all tropane alkaloids. Thus, in cocaine, this mode is predicted at 1113 cm^{-1} [27], while in both species of BZ is predicted at 1102 cm^{-1} and assigned to the weak Raman band at 1105 cm^{-1}. The N5-C6 and N5-C7 stretching modes of bicyclic rings are predicted in different regions, as in other alkaloids [18,27]. Here, the strong Raman bands at 1028 and 788 cm^{-1} are assigned to those two vibration modes. In both species of BZ, three deformations and three torsions for the benzyl (A1) and piperidine (A2) rings are expected, while only two deformations and torsions for the pyrrolidine rings, as in the free base of cocaine. Here, the redundant internal coordinates identified as β_{R1}(A2) were removed, as in cocaine, and for this reason, these coordinates for the two species of BZ are not observed in table 5 [27]. In this region, the intense Raman bands at 154, 116, 99, 53, and 33 cm^{-1} were taken from the THz spectrum of cocaine because these bands are assigned to different groups of cocaine present in both species of BZ [27].

3.8. Force constants.

Scaled internal force constants for BZ's R and S forms applying the hybrid B3LYP/6-311++G** method have been calculated from harmonic force fields with the SQMFF approach and the Molvib program [19-21]. These parameters are presented in Table 6 compared with those reported for cocaine in the same media at the B3LYP/6-31G* level of theory [27].

Table 6. Main scaled internal force constants for the R and S forms of benzoylecgonine in the gas phase and aqueous solution by using the B3LYP/6-311++G** method compared with the calculated for the free base of cocaine in the same media.

Force constant	Benzoylecgonine[a]				Cocaine[b]	
	Form R		Form S		Free base	
	Gas	Solution	Gas	Solution	Gas	Solution
f(νO-H)	7.28	7.09	7.28	7.09		
f(νN-CH₃)	4.57	4.41	4.57	4.41	4.69	4.52
f(νC-N)	4.12	3.96	4.12	3.96	4.20	4.01
f(νCH₂)	4.78	4.80	4.78	4.80	4.85	4.87
f(νCH₃)	4.67	4.74	4.67	4.74	4.86	4.92
f(νC-H)	4.98	5.02	4.98	5.02	4.86	4.91
f(νC-C)	4.94	4.95	4.94	4.95	3.94	3.98
f(δCH₂)	0.71	0.69	0.71	0.69	0.74	0.72
f(δCH₃)	0.55	0.55	0.55	0.55	0.58	0.56

Units are mdyn $Å^{-1}$ for stretching and mdyn Å rad^{-2} for angle deformations

[a]This work, [b]From Ref [27] by using B3LYP/6-31G* calculations

Analyzing first the force constants for both species of BZ, we observed that both forms present the same values, as was also observed in the vibrational analyses. In particular, the *f(νO-H)* force constants show lower values in solution, revealing that these groups are hydrated in aqueous solution, while the *f(νN-CH₃)* constants also decrease in solution because the tertiary N atoms present lone pairs that apparently are protonated in aqueous solution forming the cationic species, as in cocaine [27]. For the same reason, a decrease in the *f(νC-N)* force constants values of both BZ and cocaine are observed in the solution. In relation to the *f(νCH₂),*

f(νCH3), f(νC-H), and *f(νC-C)* force constants, we observed that the values increase slightly in solution, as observed in cocaine and scopolamine [18,27]. Here, it is necessary to clarify that the C atoms involved in those constants belong to piperidine and pyrrolidine rings, with the exception of the C atoms, which belong to the CH_3 groups (two groups in cocaine). Hence, those increases in the constants values could be attributed to bond orders that slightly increase in solution (see Table S2). The higher *f(νCH3)* and *f(δCH3)* force constants values in cocaine are attributed to the two groups, while the species of BZ only present only a group. Note that the *f(δCH2)* presents higher values than the corresponding to cocaine, probably due to the presence of additional CH_3 groups in cocaine.

3.8. Ultraviolet-visible spectrum.

The predicted ultraviolet spectrum of benzoylecgonine in an aqueous solution using the hybrid B3LYP/6-311++G** method compared with the experimental recorded in 0.2 N of H2SO4 solution taken from Ref [56] are shown in Figure 7.

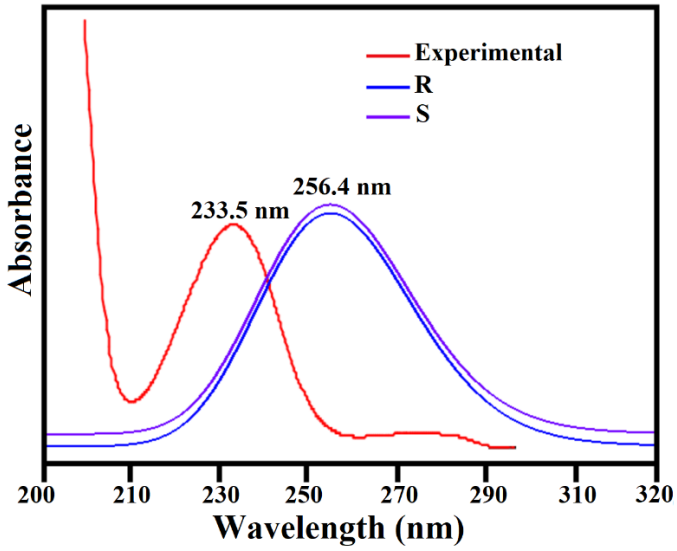

Figure 7. Comparisons between the experimental ultraviolet spectra of benzoylecgonine in 0.2 N H_2SO_4 solution [43] with those predicted for the R and S forms of the free base in aqueous solution by using the B3LYP/6-311++G** level of theory

Experimentally, one intense band and a shoulder are observed at 233.5 and 275 nm, respectively, while in the predicted spectra for both forms of benzoylecgonine, only an intense band at 256.4 is observed with band energy of 4.836 eV and oscillator strength of f=0.244. These bands are assigned to $\pi \rightarrow \pi^*$ transitions due to the presence of C=C bonds of benzyl rings and which are predicted by NBO calculations. The observed differences could be associated with the calculations because they were performed in different solutions where the interactions between solute and solvent were not considered.

4. Conclusions

In this investigation, the theoretical structures of R and S forms of the free base of benzoylecgonine were determined in the gas phase and aqueous solution using the hybrid B3LYP/6-311++G** method. Comparisons between experimental 1H- and 13C-NMR, IR, Raman, and ultraviolet spectra with the corresponding predicted by calculations show that the level of theory performs very good concordances among them while the same vibrational assignments observed for the R and S forms indicate that both species are probably present in

the solid phase and aqueous solution. The highest positive MK and NPA charges on H35 atoms of O2-H35 groups show that these atoms are the most labile than the others, as supported by the low MEP values. NPA charges on N5 of both forms decrease in solution, indicating that these atoms could be hydrated in this medium. NBO calculations show that the two forms are less stable in aqueous solution, while the gap values suggest that both species are less reactive in solution, but both most reactive than cocaine, heroin, morphine, and scopolamine in both media. Here, scaled internal force constants and complete assignments of the 114 vibration normal modes expected for those two species of benzoylecgonine are reported for the first time. The force constants related to OH and N-CH3 groups decrease in solution, revealing that the two species are hydrated in solution.

Funding

This work was supported with grants from CIUNT Project Nº 26/D608 (Consejo de Investigaciones, Universidad Nacional de Tucumán).

Acknowledgments

The authors would like to thank Prof. Tom Sundius for his permission to use MOLVIB.

Conflicts of Interest

The authors declare no conflict of interest.

References

1. Wang, J.; Deng, X.; Wu, Y.; Huang, Y.; Hou, S.; Zhang, Y.; Qiu, T.; Tong, J.; Chen, X. Sub-lethal toxicity and elimination of the cocaine metabolite, benzoylecgonine: a narrative review. *Ann. Palliat. Med.* **2021**, *10*, 6936-6947, https://doi.org/10.21037/apm-21-243.
2. Chen, X.; Deng, X.; Zhang, Y.; Wu, Y.; Yang, K.; Li, Q.; Wang, J.; Yao, W.; Tong, J. ; Xie, T.; Hou, S.; Yao, J. Computational design and crystal structure of a highly efficient benzoylecgonine hydrolase. *Angew. Chem. Int.* **2021**, *60*, 21959–21965, https://doi.org/10.1002/anie.202108559
3. Recommended Methods for the Identification and Analysis of Cocaine in Seized Materials (Revised and updated), Manual for use by National drug analysis laboratories, UNOCOD (United Nations Office on Drugs and Crime). United Nations, New York, **2012**, https://www.unodc.org/unodc/en/scientists/recommended-methods-for-the-identification-and-analysis-of-cocaine-in-seized-materials.html.
4. Montes de Oca Porto, R.; Correa Vidal, T.; Martínez Brito, D.; González Hernández, S.Y.; Terrero, O.L.; Granda Fraga, M. Development and validation of an analytical method for the simultaneous determination of benzoylecgonine and ecgonine methyl ester in human urine by gas chromatography/mass spectrometry. *Lat. Am. J. Pharm.* **2010**, *29*, 795-799, http://sedici.unlp.edu.ar/handle/10915/7984
5. Chen, X.; Zheng, X.; Zhan, M.; Zhou, Z.; Zhan, C.-G.; Zheng, F. Metabolic Enzymes of Cocaine Metabolite Benzoylecgonine, *ACS Chem Biol.* **2016**, *11*, 2186–2194, https://doi.org/10.1021/acschembio.6b00277.
6. Tan, K.; Zhou, M.; Ahrendt, A.J.; Duke, N.E.C.; Tabaja, N.; Ball, W.J.; Kirley, T.L.; Norman, A.B.; Joachimiak, A.; Schiffer, M.; Wilton, R.; Pokkuluri, P.R. Structural analysis of free and liganded forms of the Fab fragment of a high-affinity anti-cocaine antibody, h2E2. *Acta Cryst.* **2019,** *F75*, 697-706, https://doi.org/10.1107/S2053230X19013608.
7. Pedersoli, S.; Lombardi, L.; Hoëhr, N.F.; Rittner, R. Assignments of ^{1}H and ^{13}C NMR spectral data for benzoylecgonine, a cocaine metabolite. *Spectroscopy Letters* **2008**, *41*, 101-103, https://doi.org/10.1080/00387010701799696.
8. Patel, R.C.; Dutta, D.; Schonfeld, S.A. Free-base cocaine use associated with bronchiolitis obliterans organizing pneumonia. *Ann Intern Med.* **1987**, *107*, 186-187, https://doi.org/10.7326/0003-4819-107-2-186

9. Ryder, A.G.; O'Connor, G.M.; Glynn, J.T. Quantitative analysis of cocaine in solid mixtures using Raman spectroscopy and chemometric methods. *Journal of Raman Spectroscopy* **2000**, *31*, 221-227, https://doi.org/10.1002/(SICI)1097-4555(200003)31:3<221::AID-JRS518>3.0.CO;2-5.
10. Pan, Y.; Gao, D.; Yang, W.; Cho, H.; Yang, G.; Tai, H-H.; Zhan, C-G. Computational redesign of human butyrylcholinesterase for anticocaine medication. *PNAS* **2005**, *102*, 16656–16661, https://doi.org/10.1073/pnas.0507332102.
11. Davies, A.G.; Burnett, A.D.; Fan, W.; Linfield, E.H.; Cunningham, J.E. Terahertz spectroscopy of explosives and drugs. *Materials Today* **2008**, *11*, 18-26, https://doi.org/10.1016/S1369-7021(08)70016-6
12. Maharaj, R. Quantitative Analysis of Cocaine Using Fourier Transform Infrared Spectroscopy-Attenuated Total Reflectance: A Preliminary Investigation. *The Internet Journal of Third World Medicine* **2008**, *7*,1-5, http://print.ispub.com/api/0/ispub-article/8635
13. Rodrigues, N.V.S.; Cardoso, E.M.; Andrade, M.V.O.; Donnicia, C.L.; Sena, M.M. Analysis of Seized Cocaine Samples by using Chemometric Methods and FTIR Spectroscopy. *J. Braz. Chem. Soc.* **2013,** *24*, 507-517, https://doi.org/10.5935/0103-5053.20130066
14. Penido, C.A.; Pacheco, M.T.; Zângaro, R.A.; Silveira Jr., L. Identification of different forms of cocaine and substances used in adulteration using near-infrared Raman spectroscopy and infrared absorption spectroscopy. *J Forensic Sci.* **2015**, *60*, 171-178, https://doi.org/10.1111/1556-4029.12666.
15. Singh Bumbrah, G.; Sharma, R.M. Raman spectroscopy – Basic principle, instrumentation and selected applications for the characterization of drugs of abuse. *Egypt. J. Forensic Sci.* **2016**, *6*, 209-215, https://doi.org/10.1016/J.EJFS.2015.06.001.
16. Hrynchuk, R.J.; Barton, R.J.; Robertson, B.E. The crystal structure of free base cocaine, $C_{17}H_{21}NO_4$. *Can. J. Chem.* **1983**, *61*, 481-483, https://doi.org/10.1139/v83-085. .
17. Wood, M.R.; Brettell, T.A.; Thompson, H.W.; Lalancette R.A. The hydrochloride salt of L-ecgonine, a congener of cocaine. *Acta Cryst.* **2008**, *E64*, o525, https://doi.org/10.1107/S1600536808002535
18. Rudyk, R.A.; Checa, M.A.; Catalán, C.A.N.; Brandán, S.A. Structural, FT-IR, FT-Raman and ECD studies on the free base, cationic and hydrobromide species of scopolamine alkaloid. *J. Mol. Struct.* **2019**, *1180*, 603-617, https://doi.org/10.1016/j.molstruc.2018.12.040
19. Pulay, P.; Fogarasi, G.; Pongor, G.; Boggs, J.E.; Vargha, A. Combination of theoretical ab initio and experimental information to obtain reliable harmonic force constants. Scaled quantum mechanical (QM) force fields for glyoxal, acrolein, butadiene, formaldehyde, and ethylene. *J. Am. Chem. Soc.* **1983**, *105*, 7073-7047, https://doi.org/10.1021/ja00362a005
20. Rauhut, G.; Pulay, P. Transferable Scaling Factors for Density Functional Derived Vibrational Force Fields. *J. Phys. Chem*. **1995**, *99*, 3093-3100, https://doi.org/10.1021/j100010a019
21. Sundius, T. Scaling of ab-initio force fields by MOLVIB. *Vib. Spectrosc.* **2002**, *29*, 89-95, https://doi.org/10.1016/S0924-2031(01)00189-8
22. Becke, A.D. Density-functional exchange-energy approximation with correct asymptotic behavior. *Phys. Rev.* **1988**, *A38*, 3098-3100, https://doi.org/10.1103/PhysRevA.38.3098
23. Lee, C.; Yang, W.; Parr, R.G. Development of the Colle-Salvetti correlation-energy formula into a functional of the electron density. *Phys. Rev*. **1988**, *B37*, 785-789, https://doi.org/10.1103/physrevb.37.785
24. Sweta, V.R.; Lakshmi, T. Pharmacological profile of tropane alkaloids, *J. Chem. Pharm. Res.* **2015**, *7*, 117-119, https://www.jocpr.com/articles/pharmacological-profile-of-tropane-alkaloids.pdf
25. Veber, D.F.; Johnson, S.R.; Cheng, H-Y.; Brian, R.; Ward, K.W.; Kopple, K.D. Molecular Properties that influence the oral bioavailability of drug candidates. *J. Med. Chem.* **2002**, *45*, 2615-2623, https://pubs.acs.org/doi/10.1021/jm020017n
26. Lipinski, C.A.; Lombardo, F.; Dominy, B.W.; Feeney, P.J. Experimental and computational approaches to estimate solubility and permeability in drug discovery and development setting. *Advanced Drug Delivery Reviews* **2001**, *46*, 3-26, https://doi.org/10.1016/S0169-409X(00)00129-0
27. Romani, D.; Brandán, S.A. Vibrational analyses of alkaloid cocaine as free base, cationic and hydrochloride species based on their internal coordinates and force fields. *Paripex - Indian J. Res.* **2017**, *6* , 587-602.
28. Nielsen, A.B.; Holder, A.J. Gauss View 5.0, User's Reference, GAUSSIAN Inc., Pittsburgh, PA, **2008**, https://www.scirp.org/(S(vtj3fa45qm1ean45vvffcz55))/reference/ReferencesPapers.aspx?ReferenceID=1379504.
29. Frisch, M.J.; Trucks, G.W.; Schlegel, H.B.; Scuseria, G.E.; Robb, M.A.; Cheeseman, J.R.; Scalmani, G.; Barone, V.; Mennucci, B.; Petersson, G.A. Gaussian 09, Revision A.02, M. Gaussian, Inc., Wallingford CT, **2009**.

30. Miertus, S.; Scrocco, E.; Tomasi, J. Electrostatic interaction of a solute with a continuum. A direct utilization of AB initio molecular potentials for the prevision of solvent effects. *Chem. Phys.* **1981**, *55*, 117–129, https://doi.org/10.1016/0301-0104(81)85090-2
31. Tomasi, J.; Persico, J. Molecular Interactions in Solution: An Overview of Methods Based on Continous Distributions of the Solvent. *Chem. Rev.* **1994**, *94*, 2027-2094, https://doi.org/10.1021/cr00031a013.
32. Marenich, A.V.; Cramer, C.J.; Truhlar, D.G. Universal solvation model based on solute electron density and a continuum model of the solvent defined by the bulk dielectric constant and atomic surface tensions. *J. Phys. Chem.* **2009**, *B113*, 6378-6396, https://doi.org/10.1021/jp810292n.
33. Ugliengo, P. Moldraw Program, University of Torino, Dipartimento Chimica IFM, Torino, Italy, **1998**.
34. Besler, B.H.; Merz, J.K.M.; Kollman, P.A. Atomic charges derived from semiempirical methods. *J. Comp. Chem.* **1990**, *11*, 431-439, https://doi.org/10.1002/jcc.540110404
35. Glendening, E.D.; Badenhoop, J.K.; Reed, A.D.; Carpenter, J.E.; Weinhold, F. NBO 3.1; Theoretical Chemistry Institute, University of Wisconsin; Madison, WI. **1996**.
36. Bader, R.F.W. Atoms in Molecules, A Quantum Theory. Oxford University Press, Oxford, **1990**, https://www.scirp.org/(S(vtj3fa45qm1ean45vvffcz55))/reference/referencespapers.aspx?referenceid=1379502.
37. Biegler-Köning, F.; Schönbohm, J.; Bayles, D. AIM2000; A Program to Analyze and Visualize Atoms in Molecules. *J. Comput. Chem.* **2001**, *22*.
38. Ditchfield, R. Self-consistent perturbation theory of diamagnetism. I. A gage-invariant LCAO (linear combination of atomic orbitals) method for NMR chemical shifts. *Mol Phys.* **1974**, *27*, 714–722, https://doi.org/10.1080/00268977400100711
39. Pauling, P.; Datta, N. Anticholinergic substances: A single consistent conformation. *Proc. NatI. Acad. Sci*. **1980**, *77*, 708-712, https://doi.org/10.1073%2Fpnas.77.2.708
40. Available from Web page: https://spectrabase.com/spectrum
41. Keresztury, G.; Holly, S.; Besenyei, G.; Varga, J.; Wang, A.Y.; Duri, J.R. Vibrational spectra of monothiocarbamates-II. IR and Raman spectra, vibrational assignment, conformational analysis and ab initio calculations of S-methyl-N,N-dimethylthiocarbamate. *Spectrochim. Acta* **1993,** *49A*, 2007-2026, https://doi.org/10.1016/S0584-8539(09)91012-1
42. Davies, A.G.; Burnett, A.D.; Fan, W.; Linfield, E.H.; Cunningham, J.E. Terahertz spectroscopy of explosives and drugs, *Materials Today* **2008**, *11*, 18-26, https://doi.org/10.1016/S1369-7021(08)70016-6
43. Ruiz Hidalgo, J.; Brandán, S.A. Theoretical DFT Studies on Free base, Cationic and Hydrochloride species of Narcotic Tramadol Agent in Gas Phase and Aqueous Solution., *Biointerface Research in Applied Chemistry* **2021**, *11*, 13064-13088, https://doi.org/10.33263/BRIAC115.1306413088
44. Karrouchi, K.; Mortada, S.; Issaoui, N.; El-gourrami, O.; Arshad, S.; Benzeid, H.; Sagaama, A.; El Karbane, M.; Faouzi, M.E.A.; Brandán, S.A. Synthesis, crystal structure, spectroscopic, antidiabetic, antioxidant and computational investigations of Ethyl 5-hydroxy-1-isonicotinoyl-3-methyl-4,5-dihydro-1H-pyrazole-5-carboxylate, *J Mol. Struct*. **2022**, *1251*, 131977, https://doi.org/10.1016/j.molstruc.2021.131977
45. Karrouchi, K.; Brandán, S.A.; Sert, Y.; El Karbane, M.; Radi, S.; Ferbinteanu, M.; Garcia, Y.; Ansar, M. Synthesis, structural, molecular docking and spectroscopic studies of (E)-N'-(4-methoxybenzylidene)-5-methyl-1H-pyrazole-3-carbohydrazide. *J Mol. Struct.* **2021**, *1225*, 129072, https://doi.org/10.1016/j.molstruc.2020.129072
46. El Kalai, F.; Karrouchi, K.; Baydere, C.; Daoui, S.; Allali, M.; Dege, N.; Benchat, N.; Brandán, S.A. Synthesis, crystal structure, spectroscopic studies, NBO, AIM and SQMFF calculations of new pyridazinone derivative. *J Mol. Struct.* **2021**, *1223*, 129213, https://doi.org/10.1016/j.molstruc.2020.129213
47. Karrouchi, K.; Brandán, S.A.; Hassan, M.; Bougrin, K.; Radi, S.; Ferbinteanu, M.; Garcia, Y.; Ansar, M. Synthesis, X-ray, spectroscopy, molecular docking and DFT calculations of (E)-N'-(2,4-dichlorobenzylidene)-5-phenyl-1H-pyrazole-3-carbohydrazide. *J Mol. Struct*. **2021**, *1228*, 129714, https://doi.org/10.1016/j.molstruc.2020.129714
48. Iramain, M.A.; Ruiz Hidalgo, J.; Sundius, T.; Brandán, S.A. A Combined Study on Structures and Vibrational Spectra of Antiviral Rimantadine using SQMFF and DFT calculations. *Heliyon 8*, **2022,** e10102. https://doi.org/10.1016/j.heliyon.2022.e10102
49. Darugar, V.; Vakili, M.; Manzur, M.E.; Brandán, S.A.Structural and vibrational investigation of Cis-Trans isomers of potent insecticide allethrin. *J. Molec. Modeling* **2022**, *28*, 268, https://doi.org/10.1007/s00894-022-05272-y

50. Vakili, M.; Romano, E.; Darugar, V.; Brandán, S.A. Behaviors of Antiviral Oseltamivir in different media. DFT and SQMFF Calculations. *J. Mol. Model.* **2021**, *27*, 237, https://doi.org/10.1007/s00894-021-04962-3
51. Laurella, L.C.; Ruiz Hidalgo, J.; Catalán, C.A.N.; Sülsen, V.P.; Brandán, S.A. Structure and absolute configuration of parodiolide, a new dimeric sesquiterpene lactone isolated from Mikania parodii Cabrera possessing an uncommon spiro connexion. *J Mol. Struct.* **2022**, *1253*, 132270, https://doi.org/10.1016/j.molstruc.2021.132270
52. Assenine, M.A.; Haddad, B.; Paolone, A.; Brandán, S.A.; Goussem, M.; Villemin, D.; Boumediene, M.; Rahmouni, M.; Bresson, S. Synthesis, thermal properties, vibrational spectra and computational studies of Trioctylmethylammonium bis (trifluoromethylsulfonyl) imide ionic liquid. *J Mol. Struct.* **2021**, *1232*, 130085, https://doi.org/10.1016/j.molstruc.2020.129625
53. Fetouhi, B.; Haddad, B.; Brandán, S.A.; Paolone, A.; Villemin, D.; Boumediene, M.; Rahmouni, M.; Bresson, S. Synthesis, molecular structure, and properties of DABCO bromide based ionic liquid combining spectroscopic studies with DFT calculations. *J Mol. Struct.* **2021,** *1233*, 130102, https://doi.org/10.1016/j.molstruc.2022.132682
54. Iramain, M.A.; Imbarack, E.; Leyton Bongiorno, P.; Lizarraga, E.; Brandán, S.A. Solvation of Potassium 5-Hydroxy Pentanoyl Trifluoroborate Salt in Aqueous Environment by Using FT-Raman and UV-Visible Spectra. *Biointerface Research in Applied Chemistry*, **2022**, *12(2)*, 2196 – 2215. https://doi.org/10.33263/BRIAC122.21962215
55. Gatfaoui, S.; Issaoui, N.; Brandán, S.A.; Medimagh, M.; Al-Dossary, O.; Roisnel, T.; Marouani, H.; Kazachenko, A.S. Deciphering non-covalent interactions of 1,3-Benzenedimethanaminium bis(trioxonitrate): Synthesis, empirical and computational study. *J Mol. Struct.* **2022**, *1250*, 131720, https://doi.org/10.1016/j.molstruc.2021.131720
56. Available from Web page: https://www.sigmaaldrich.cn/deepweb/assets/sigmaaldrich/product/documents/260/735/b8900-74k8801dat.pdf

Supplementary Data

Table S1. Atomic MK charges and molecular electrostatic potentials for R and S form of benzoylecgonine by using the hybrid B3LYP/6-311++G** level of theory.

Atoms	MK charges				MEP			
	R Form		S Form		R Form		S Form	
	Gas	Solution	Gas	Solution	Gas	Solution	Gas	Solution
1 O	-0.473	-0.459	-0.490	-0.488	-22.329	-22.327	-22.323	-22.327
2 O	-0.632	-0.650	-0.640	-0.657	-22.324	-22.321	-22.324	-22.321
3 O	-0.563	-0.588	-0.565	-0.587	-22.383	-22.387	-22.383	-22.386
4 O	-0.553	-0.563	-0.557	-0.562	-22.387	-22.390	-22.387	-22.390
5 N	-0.254	-0.287	-0.243	-0.276	-18.403	-18.403	-18.403	-18.403
6 C	-0.087	0.006	-0.068	-0.068	-14.730	-14.728	-14.730	-14.728
7 C	0.205	0.196	0.171	0.229	-14.737	-14.738	-14.737	-14.738
8 C	-0.168	-0.218	-0.122	-0.100	-14.748	-14.747	-14.748	-14.747
9 C	-0.047	-0.126	-0.092	-0.113	-14.769	-14.768	-14.769	-14.768
10 C	-0.206	-0.207	-0.154	-0.207	-14.771	-14.770	-14.771	-14.770
11 C	-0.599	-0.598	-0.536	-0.550	-14.775	-14.774	-14.775	-14.774
12 C	0.579	0.539	0.582	0.598	-14.704	-14.701	-14.704	-14.702
13 C	-0.393	-0.402	-0.483	-0.473	-14.751	-14.752	-14.751	-14.752
14 C	0.723	0.788	0.718	0.758	-14.642	-14.643	-14.643	-14.643
15 C	0.587	0.607	0.608	0.576	-14.645	-14.645	-14.645	-14.645
16 C	0.060	0.039	0.039	0.086	-14.757	-14.755	-14.757	-14.755
17 C	-0.146	-0.151	-0.144	-0.156	-14.767	-14.766	-14.766	-14.766
18 C	-0.183	-0.180	-0.169	-0.192	-14.766	-14.765	-14.766	-14.765
19 C	-0.116	-0.130	-0.122	-0.132	-14.767	-14.767	-14.767	-14.767
20 C	-0.094	-0.103	-0.106	-0.113	-14.767	-14.767	-14.767	-14.767
21 C	-0.138	-0.100	-0.118	-0.112	-14.763	-14.763	-14.763	-14.763
22 H	0.148	0.126	0.143	0.139	-1.111	-1.109	-1.111	-1.109
23 H	0.094	0.100	0.096	0.084	-1.115	-1.116	-1.115	-1.116
24 H	0.102	0.110	0.085	0.077	-1.101	-1.103	-1.101	-1.103
25 H	0.026	0.048	0.069	0.079	-1.116	-1.115	-1.119	-1.118
26 H	0.061	0.079	0.034	0.042	-1.119	-1.118	-1.116	-1.115
27 H	0.068	0.077	0.056	0.068	-1.121	-1.120	-1.118	-1.117
28 H	0.068	0.074	0.057	0.073	-1.118	-1.117	-1.121	-1.120
29 H	0.194	0.205	0.125	0.124	-1.128	-1.127	-1.120	-1.120
30 H	0.143	0.146	0.177	0.178	-1.120	-1.120	-1.128	-1.127
31 H	0.063	0.075	0.052	0.053	-1.111	-1.109	-1.111	-1.109
32 H	0.139	0.148	0.155	0.153	-1.116	-1.115	-1.120	-1.120
33 H	0.130	0.133	0.163	0.166	-1.121	-1.120	-1.115	-1.115
34 H	0.153	0.156	0.175	0.174	-1.115	-1.115	-1.115	-1.115
35 H	0.430	0.435	0.432	0.440	-0.961	-0.957	-0.961	-0.957
36 H	0.137	0.146	0.137	0.144	-1.106	-1.106	-1.106	-1.106
37 H	0.168	0.163	0.165	0.165	-1.107	-1.105	-1.107	-1.105
38 H	0.125	0.128	0.125	0.131	-1.103	-1.102	-1.103	-1.102
39 H	0.117	0.119	0.119	0.126	-1.103	-1.103	-1.103	-1.103
40 H	0.132	0.118	0.126	0.125	-1.100	-1.100	-1.100	-1.100

Table S2. NPA charges and Wiberg indexes for R and S form of benzoylecgonine in gas phase and aqueous solution by using the hybrid B3LYP/6-311++G** level of theory.

Atoms	NPA charges				Wiberg indexes			
	R Form		S Form		R Form		S Form	
	Gas	Solution	Gas	Solution	Gas	Solution	Gas	Solution
1 O	-0.556	-0.556	-0.556	-0.556	2.167	2.170	2.167	2.170
2 O	-0.699	-0.693	-0.699	-0.693	1.967	1.977	1.967	1.977
3 O	-0.592	-0.596	-0.592	-0.596	2.047	2.033	2.047	2.033
4 O	-0.613	-0.619	-0.613	-0.619	2.006	1.994	2.006	1.995
5 N	-0.574	-0.566	-0.574	-0.566	3.089	3.082	3.089	3.082
6 C	0.002	0.004	0.002	0.004	3.934	3.937	3.934	3.937

Atoms	NPA charges				Wiberg indexes			
	R Form		S Form		R Form		S Form	
	Gas	Solution	Gas	Solution	Gas	Solution	Gas	Solution
7 C	-0.008	-0.010	-0.008	-0.010	3.936	3.937	3.936	3.937
8 C	-0.338	-0.338	-0.338	-0.338	3.973	3.974	3.973	3.974
9 C	-0.415	-0.416	-0.415	-0.416	3.929	3.928	3.929	3.928
10 C	-0.414	-0.416	-0.414	-0.416	3.931	3.930	3.931	3.930
11 C	-0.400	-0.401	-0.400	-0.401	3.928	3.928	3.928	3.928
12 C	0.126	0.131	0.126	0.131	3.859	3.856	3.859	3.856
13 C	-0.355	-0.359	-0.355	-0.359	3.853	3.855	3.853	3.855
14 C	0.830	0.824	0.830	0.824	3.835	3.839	3.835	3.839
15 C	0.802	0.800	0.802	0.800	3.840	3.840	3.840	3.841
16 C	-0.159	-0.160	-0.159	-0.160	4.004	4.004	4.004	4.004
17 C	-0.154	-0.152	-0.154	-0.152	3.954	3.954	3.954	3.954
18 C	-0.157	-0.156	-0.157	-0.156	3.951	3.953	3.951	3.953
19 C	-0.207	-0.207	-0.207	-0.207	3.965	3.965	3.965	3.965
20 C	-0.206	-0.206	-0.206	-0.206	3.965	3.965	3.965	3.965
21 C	-0.179	-0.178	-0.179	-0.178	3.966	3.966	3.966	3.966
22 H	0.220	0.216	0.220	0.216	0.954	0.956	0.954	0.956
23 H	0.207	0.206	0.207	0.206	0.959	0.959	0.959	0.959
24 H	0.249	0.246	0.249	0.246	0.941	0.943	0.941	0.943
25 H	0.211	0.211	0.208	0.208	0.958	0.958	0.959	0.959
26 H	0.208	0.208	0.211	0.211	0.959	0.959	0.958	0.958
27 H	0.205	0.206	0.206	0.206	0.960	0.960	0.960	0.960
28 H	0.206	0.206	0.205	0.206	0.960	0.960	0.960	0.960
29 H	0.235	0.237	0.206	0.205	0.948	0.947	0.960	0.960
30 H	0.206	0.205	0.235	0.237	0.960	0.961	0.948	0.947
31 H	0.207	0.208	0.207	0.208	0.961	0.961	0.961	0.961
32 H	0.197	0.197	0.161	0.162	0.963	0.963	0.978	0.978
33 H	0.161	0.162	0.197	0.197	0.978	0.978	0.963	0.963
34 H	0.196	0.196	0.196	0.196	0.963	0.964	0.963	0.963
35 H	0.482	0.485	0.482	0.485	0.772	0.769	0.772	0.769
36 H	0.227	0.228	0.227	0.228	0.951	0.950	0.951	0.950
37 H	0.232	0.229	0.232	0.229	0.948	0.949	0.948	0.950
38 H	0.207	0.207	0.207	0.207	0.959	0.959	0.959	0.959
39 H	0.207	0.207	0.207	0.207	0.959	0.959	0.959	0.959
40 H	0.205	0.205	0.205	0.205	0.960	0.960	0.960	0.960

Table S3. Main donor-acceptor energy interactions (in kJ/mol) for R an S forms of benzoylecgonine in gas phase and aqueous solution by using the hybrid B3LYP/6-311++G** level of theory.

Delocalization	Benzoilecgonine			
	R Form		S Form	
	Gas	Solution	Gas	Solution
π (2)C16-C18→π*O4-C15	91.25	93.34	91.25	93.34
π (2)C16-C18→π*C17-C19	88.03	87.45	88.03	87.45
π (2)C16-C18→π*C20-C21	77.08	77.12	77.08	77.12
π (2)C17-C19→π*C16-C18	79.21	78.71	79.21	78.71
π (2)C17-C19→π*C20-C21	90.71	90.83	90.71	90.83
π (2) C20-C21→π* C16-C18	93.80	94.30	93.80	94.30
π (2) C20-C21→π* C17-C19	76.08	75.70	76.08	75.70
$\Delta ET_{\pi\rightarrow\pi^*}$	**596.15**	**597.45**	**596.15**	**597.45**
π*O4-C15→π* C16-C18	445.13	418.29	445.38	418.50
$\Delta ET_{\pi^*\rightarrow\pi^*}$	**445.13**	**418.29**	**445.38**	**418.50**
LP(2)O3 → σ*O2-C14	145.38	136.94	145.38	136.94
LP(2)O3 → σ*C8-C14	76.95	72.52	76.95	72.48
LP(2)O4 → σ*O1-C15	131.59	125.73	131.59	125.78

Delocalization	Benzoilecgonine			
	R Form		S Form	
	Gas	Solution	Gas	Solution
*LP(2)O4 → σ*C15-C16*	71.52	69.22	71.56	69.22
$\Delta ET_{LP\rightarrow\sigma^*}$	**425.44**	**404.42**	**425.48**	**404.42**
*LP(2)O1 → π*O4-C15*	193.28	199.80	193.28	199.76
*LP(2)O2 → π*O3-C14*	175.73	183.71	175.73	183.67
$\Delta ET_{LP\rightarrow\pi^*}$	**369.01**	**383.52**	**369.01**	**383.43**
ΔE_{Total}	**1835.73**	**1803.67**	**1836.02**	**1803.79**

Table S4. Analysis of the topological properties for R an S forms of benzoylecgonine by using the hybrid B3LYP/6-311++G** level of theory.

R form					
Gas phase					
Parameter (a.u.)	**O3---H29**	RCPN	RCP1	RCP2	RCP3
$\rho(r_c)$	0.0078	0.0078	0.0218	0.0205	0.0415
$\nabla^2\rho(r_c)$	0.0284	0.0316	0.1600	0.1252	0.2496
λ_1	-0.0059	-0.0051	-0.0172	-0.0143	-0.0429
λ_2	-0.0023	0.0027	0.0878	0.0606	0.1454
λ_3	0.0365	0.0341	0.0893	0.0788	0.1471
$\lvert\lambda_1\rvert/\lambda_3$	0.1616	0.1496	0.1926	0.1815	0.2916
Distance (Å)	*2.666*				
Aqueous solution					
Parameter (a.u.)	**O3---H29**	RCPN	RCP1	RCP2	RCP3
$\rho(r_c)$	0.0072	0.0072	0.0218	0.0204	0.0416
$\nabla^2\rho(r_c)$	0.0268	0.0280	0.1592	0.1228	0.2488
λ_1	-0.0054	-0.0051	-0.0171	-0.0146	-0.0431
λ_2	-0.0011	0.0011	0.0871	0.0590	0.1439
λ_3	0.0332	0.0321	0.0893	0.0783	0.1481
$\lvert\lambda_1\rvert/\lambda_3$	0.1626	0.1589	0.1915	0.1865	0.2910
Distance (Å)	*2.722*				
S form					
Gas phase					
Parameter (a.u.)	**O3---H30**	RCPN	RCP1	RCP2	RCP3
$\rho(r_c)$	0.0078	0.0078	0.0218	0.0205	0.0415
$\nabla^2\rho(r_c)$	0.0284	0.0316	0.1600	0.1252	0.2496
λ_1	-0.0059	-0.0051	-0.0172	-0.0143	-0.0429
λ_2	-0.0023	0.0027	0.0878	0.0606	0.1454
λ_3	0.0365	0.0341	0.0893	0.0788	0.1471
$\lvert\lambda_1\rvert/\lambda_3$	0.1616	0.1496	0.1926	0.1815	0.2916
Distance (Å)	*2.666*				
Aqueous solution					
Parameter (a.u.)	**O3---H30**	RCPN	RCP1	RCP2	RCP3
$\rho(r_c)$	0.0072	0.0072	0.0218	0.0204	0.0416
$\nabla^2\rho(r_c)$	0.0268	0.0280	0.1592	0.1228	0.2488
λ_1	-0.0054	-0.0051	-0.0171	-0.0146	-0.0431
λ_2	-0.0011	0.0012	0.0871	0.0590	0.1438
λ_3	0.0332	0.0322	0.0893	0.0783	0.1481
$\lvert\lambda_1\rvert/\lambda_3$	0.1626	0.1583	0.1915	0.1865	0.2910
Distance (Å)	*2.722*				

Table S5. Calculated HOMO and LUMO orbitals, energy band gap, chemical potential (μ), electronegativity (χ), global hardness (η), global softness (S), global electrophilicity index (ω) and global nucleophilicity index (E) for R an S forms of benzoylecgonine by using the hybrid B3LYP/6-311++G** level of theory.

Frontier orbitals (eV)	**R Form**		**S Form**	
	Gas	Solution	Gas	Solution
HOMO	-6.2823	-6.3468	-6.2820	-6.3470
LUMO	-1.5426	-1.5755	-1.5426	-1.5760
|GAP|	**4.7397**	**4.7712**	**4.7394**	**4.7710**
Descriptors (eV)				
χ	3.9124	3.9611	3.9123	3.9615
μ	-3.9124	-3.9611	-3.9123	-3.9615
η	-1.5985	-1.5978	-1.5984	-1.5975
S	-0.3128	-0.3129	-0.3128	-0.3130
ω	-4.7879	-4.9099	-4.7880	-4.9119

χ = - [E(LUMO) - E(HOMO)]/2; μ = [E(LUMO) + E(HOMO)]/2;
η = [E(LUMO) – E(HOMO)]/2; S = ½η;ω = $\mu^2/2\eta$

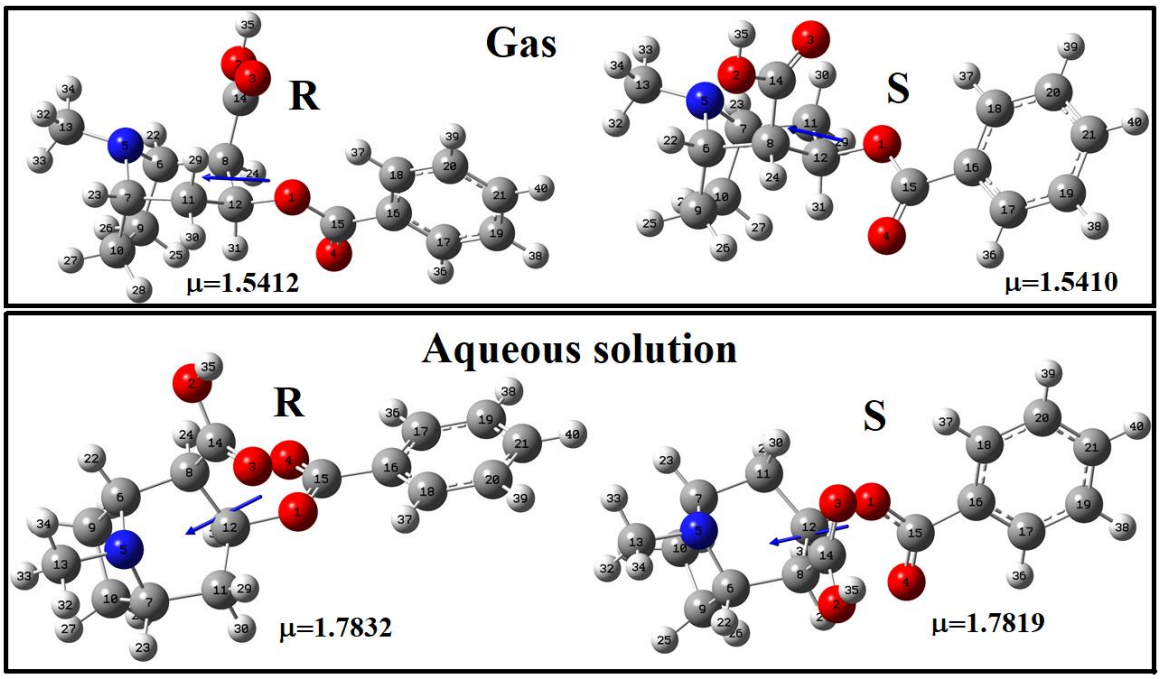

Figure S1. Dipole moment values for the for R and S forms of benzoylecgonine in gas phase and aqueous solution at the B3LYP/6-311++G** level of theory showing the corresponding magnitudes and orientations of their vectors.

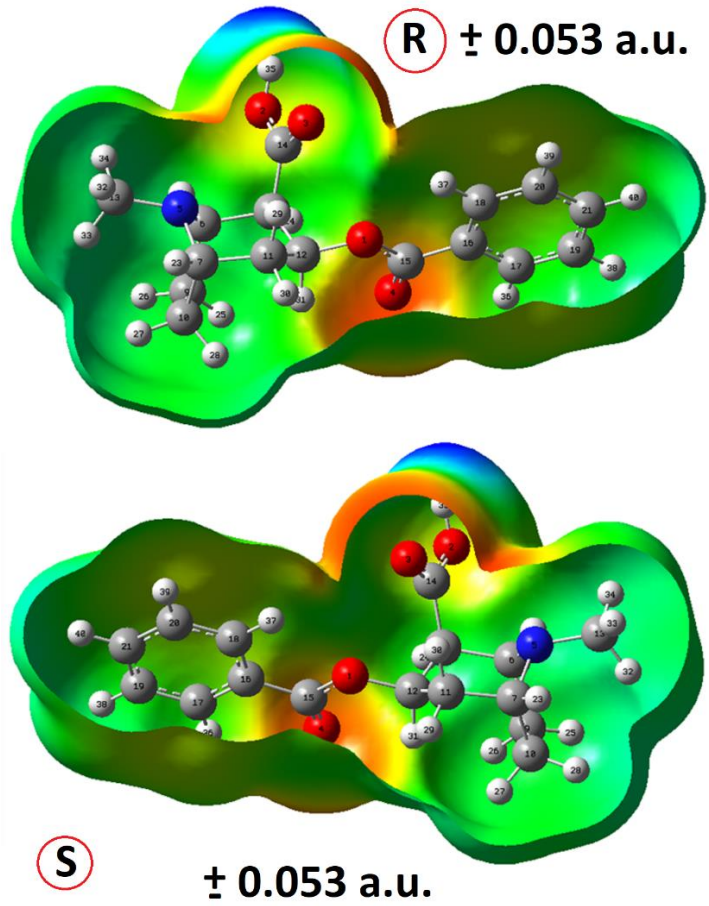

Figure S2. Calculated electrostatic potential surfaces on the molecular surfaces of the R (upper) and S (bottom) forms of free base benzoylecgonine in gas phase. Color ranges. In au: from red -0.053 to blue +0.053. B3LYP functional and 6-31G* basis set. Isodensity value of 0.005.

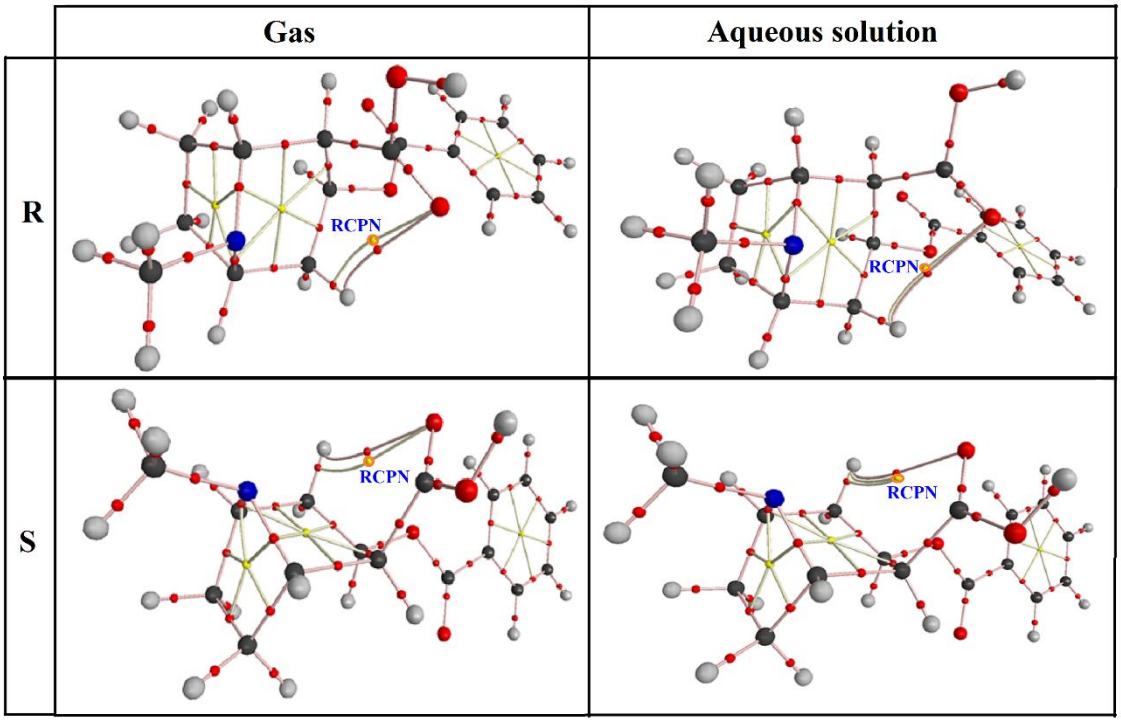

Figure S3. Molecular graphics for the R and S forms of benzoylecgonine in gas phase and aqueous solution at the B3LYP/6-311++G** level of theory showing the formation of new H bonds and RCPNs.